SOILS AND FOUNDATIONS Vol. 43, No. 3, 73-84, June 2003
Japanese Geotechnical Society

MICROSCOPIC INTERPRETATION ON A STRESS-DILATANCY RELATIONSHIP OF GRANULAR MATERIALS

SIHONG LIU[i] and HAJIME MATSUOKA[ii]

ABSTRACT

Matsuoka (1974) proposed a two-dimensional stress-dilatancy equation of granular materials on the mobilized plane through the direct box shear tests on assemblies of aluminum and photoelastic rods, which was expressed as $\tau/\sigma_N = \lambda(-d\varepsilon_N/d\gamma)+\mu$. In this paper, the stress ratio τ/σ_N and the strain increment ratio $-d\varepsilon_N/d\gamma$ are approximated to be $\tan\bar{x}$ and $\tan\bar{\theta}$, respectively, on the basis of the numerically simulated results for a simple shear test by DEM. Here, $\bar{x}$ and $\bar{\theta}$ denote the average angle of the interparticle forces to the normal of the mobilized plane and the average interparticle contact angle on the mobilized plane, respectively. It was found that the difference between $\bar{x}$ and $\bar{\theta}$, denoted as δ, varies slightly during shear. The angle δ is related to the average interparticle contact force f_0, the slope k of the straight line that characterizes the distribution of the average interparticle contact forces against the contact angle, and the average interparticle contact angles $\bar{\theta}$ on the mobilized plane. The intercept μ in the stress-dilatancy equation is interpreted as $\tan\delta$. The influences of interparticle surface friction, grain shape and confining pressure on the stress-dilatancy relation are examined. It was found that the angle δ is not very sensitive to the interparticle surface friction angle ϕ_μ, except in the lower value of ϕ_μ, and independent of the confining pressure. However, it is affected to some extent by grain shapes. Various results of the newly developed in-situ direct shear tests on various granular soils are presented to support the arguments in this paper.

Key words: distinct element method, granular materials, microscopic, simple shear test, stress-dilatancy (**IGC**: D6)

INTRODUCTION

The stress-dilatancy relation that usually specifies the direction of the plastic strain increment vector in the plasticity theory is one of the most important relations in the constitutive equation for granular materials. Rowe (1962) proposed a stress-dilatancy equation based on force equilibrium and the principle of least work for granular particles in contact. Scofield and Wroth (1968) derived a stress-dilatancy equation from considering energy dissipation, which is now applied in the Cam-clay model. Through direct box shear tests on assemblies of aluminum and photoelastic rods, Matsuoka (1974) derived a two-dimensional stress-dilatancy equation on the mobilized plane by taking the probability distribution of interparticle contact angles into account, which was expressed as $\tau/\sigma_N = \lambda(-d\varepsilon_N/d\gamma)+\mu$. This equation was latter extended to the three-dimensional stress state based on the theory of the "Spatial mobilized plane" (SMP) (Matsuoka and Nakai, 1974; Nakai and Matsuoka, 1980).

Yamamoto et al. (1994, 1995) has numerically simulated a biaxial compression test on aluminum rod mass by the distinct element method (Cundall and Strack, 1979) and examined the two-dimensional stress-dilatancy equation of granular materials derived by Matsuoka (1974) from a microscopic view on the basis of DEM simulation results. In their studies, the interparticle contact force at each contact was assumed to be the same, i.e. the probability distribution of interparticle contact forces was assumed to be analogous to that of interparticle contact angles. Further, the mobilized interparticle friction angle $\phi_{\mu mo}$ at each contact was assumed to be equal to either the interparticle friction angle, ϕ_μ, or the average magnitude of $\phi_{\mu mo}$ over all the contacts, $\bar{\phi}_{\mu mo}$. These assumptions led the intercept μ in the stress-dilatancy equation to be equal to either $\tan\phi_\mu$ or $\tan\bar{\phi}_{\mu mo}$. In this study, we simulate a simple shear test on aluminum rod mass by DEM and then re-examine Matsuoka's two-dimensional stress-dilatancy equation based on the simulation results. In this study, we take the real interparticle contact force and mobilized interparticle friction angle for each contact into consideration. Moreover, the intercept μ in this stress-dilatancy equation is interpreted from a microscopic point of view and the influences of interparticle friction, grain shape and confining pressure on the intercept are investigated.

[i] Research Fellow, Department of Civil Engineering, Nagoya Institute of Technology, Gokiso-cho, Showa-ku, Nagoya 466-8555, Japan.
[ii] Professor, ditto.
Manuscript was received for review on May 9, 2002.
Written discussions on this paper should be submitted before January 1, 2004 to the Japanese Geotechnical Society, Sugayama Bldg. 4F, Kanda Awaji-cho 2-23, Chiyoda-ku, Tokyo 101-0063, Japan. Upon request the closing date may be extended one month.

NUMERICAL SIMULATION FOR A SIMPLE SHEAR TEST BY DEM

Figure 1 shows a simple shear test on an assembly of aluminum rods which models a two-dimensional granular material. The aluminum rods in the assembly are 50 mm long and have the diameters of 3 mm and 5 mm with a mixing ratio of 3:2 by weight. The advantage of using aluminum rods is that its specific gravity (2.69) is close to soil particles' gravity (2.65). In the testing setup, two rigid lateral platens are connected to both the base platen and a rigid bar at the upper backside with two hinges, respectively. The geometrical configuration of this testing setup keeps the same rotation for both the left and the right lateral walls. A layer of aluminum rods is pasted with glue on both the downward surface of the upper loading platen and the upward surface of the basal platen to prevent slippage between the platens and aluminum rods. The upper loading platen on the specimen is pulled horizontally with a rope while a constant dead load is applied on the specimen, which causes the inclination of the two lateral walls and thus induces a shear strain in the specimen. This test is then numerically simulated by DEM. The computing program used in our simulation is GRADIA coded by Yamamoto (1995). The DEM specimen of 800 particles was generated by digitizing the aluminum rods from the picture of the test shown in Fig. 1. The mechanical properties of the aluminum rods are: Young's modulus $E=71$ GPa, Poisson's ratio $\nu=0.34$ and the interparticle friction angle $\phi_\mu=16°$. By using these properties, the normal and tangential (shear) stiffness between the aluminum rods are determined to be 9.0 GPa and 0.3 GPa, respectively, based on the contact theory of two elastic rigid spheres. Figure 2(a) shows the comparison of the experimental and the numerically simulated results with respect to the relationships among the shear-normal stress ratio τ/σ_N, shear stain γ and normal strain ε_N. It can be seen that the numerically simulated results (solid lines) are in good agreement with the experimental results (open circular plots), thus indicating the accuracy of the DEM simulation.

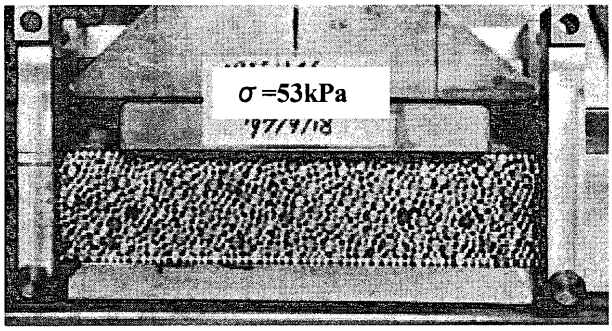

Fig. 1. Simple shear test on assembly of aluminum rods

In addition to $\phi_\mu=16°$ of the aluminum rods, the same simple shear test as shown in Fig. 1 was also simulated with $\phi_\mu=0°$, 4°, 8°, 32°, 64° while the other parameters used in the DEM simulation were kept unchanged. Their results are shown in Fig. 2(b). It is interesting to see that although the shear strength of the granular material increases with an increasing interparticle friction angle ϕ_μ, it does not increase proportionally with the increase in ϕ_μ. Figure 2(b) also shows that the dilative normal strain of the sample increases accompanying increasing ϕ_μ. In the latter part of this paper, the effects of interparticle friction angle ϕ_μ on the stress-dilatancy relationship will be investigated based on these numerical simulation results.

STRESS-DILATANCY RELATIONSHIP CORRELATED TO MICROSCOPIC VARIABLES ON MOBILIZED PLANE

Paying attention to the interparticle contacts along a mobilized plane as shown in Fig. 3 and denoting the interparticle contact angle by θ_i, the interparticle contact force by f_i and the mobilized interparticle friction angle by $\phi_{\mu moi}$, one can obtain the following equation from the equilibrium of interparticle forces on the mobilized plane.

$$\frac{\tau}{\sigma_N}=\frac{\sum_{i=1}^{n} f_i\cdot\sin(\theta_i+\phi_{\mu moi})}{\sum_{i=1}^{n} f_i\cdot\cos(\theta_i+\phi_{\mu moi})}=\frac{\sum_{i=1}^{n} f_i\cdot\sin x_i}{\sum_{i=1}^{n} f_i\cdot\cos x_i} \tag{1}$$

where n denotes the number of the interparticle contacts along the mobilized plane and $x_i(=\theta_i+\phi_{\mu moi})$ denotes the

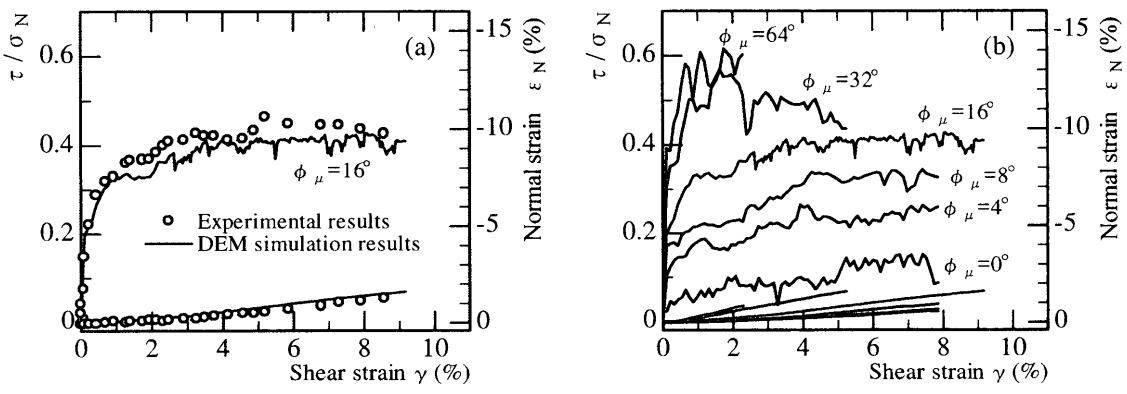

Fig. 2. Numerically simulated and experimental stress-strain relationships for a simple shear test on assembly of aluminum rods

angle between the interparticle contact force f_i and the normal to the mobilized plane. The angle x_i changes from $-\pi/2$ to $\pi/2$. Along the mobilized plane, all the interparticle forces f_i can be characterized with a probability distribution function with respect to the angle x_i, which is denoted as $F(x)$. If we replace f_i approximately with $F(x)$, then Eq. (1) can be rewritten as follows:

$$\frac{\tau}{\sigma_N}=\frac{\int_{-\pi/2}^{\pi/2}F(x)\cdot\sin x\,dx}{\int_{-\pi/2}^{\pi/2}F(x)\cdot\cos x\,dx}\cong\tan\bar{x} \tag{2}$$

where $\bar{x}=(\int_{-\pi/2}^{\pi/2}F(x)\cdot x dx)/(\int_{-\pi/2}^{\pi/2}F(x)dx)$, which may be termed as the average angle of the contact forces for convenience and is equivalent to the mobilized frictional angle ϕ_{mo}.

On the other hand, the relation between the normal-shear strain increment ratio, $-d\varepsilon_N/d\gamma$, and the average interparticle contact angle $\bar{\theta}$ is expressed as follows (Matsuoka,1974; Yamamoto, 1995):

$$-\frac{d\varepsilon_N}{d\gamma}=\frac{\int_{-\pi/2}^{\pi/2}N(\theta)\cdot\sin\theta\,d\theta}{\int_{-\pi/2}^{\pi/2}N(\theta)\cdot\cos\theta\,d\theta}\cong\tan\bar{\theta} \tag{3}$$

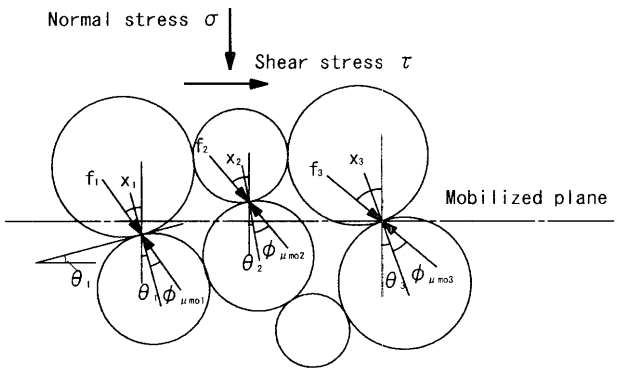

Fig. 3. Equilibrium of interparticle contact forces on mobilized plane

where $\bar{\theta}=(\int_{-\pi/2}^{\pi/2}N(\theta)\cdot\theta d\theta)/(\int_{-\pi/2}^{\pi/2}N(\theta)d\theta)$, and $N(\theta)$ denotes the probability distribution of interparticle contact angles along the mobilized plane, i.e. the number of the contacts with respect to the contact angle θ.

It should be pointed out that Eqs. (2) and (3) are statistical approximation equations, which are derived by approximating the angles x and θ with their corresponding average angles $\bar{x}$ and $\bar{\theta}$, respectively, during numerical integration along the mobilized plane. It has been verified by using the data of the DEM simulations in this paper that the error of these approximations is below 3° when $\bar{x}$ (or $\bar{\theta}$) is less than 50°. The reasonability of Eq. (3) has also been verified through the direct box shear tests on the assemblies of aluminum and photoelastic rods by Matsuoka (1974) as well as through the DEM simulation for biaxial compression tests by Yamamoto (1995).

Figure 4(a) shows the evolutions of $\bar{x}$ and $\bar{\theta}$ during shear from the numerically simulated results for the simple shear test corresponding to $\phi_\mu=16°$, and Fig. 4(b) shows the evolutions of the mean values of $\bar{x}$ and $\bar{\theta}$ over the calculated shear procedure with respect to different interparticle friction angles ϕ_μ. It is seen from Fig. 4(a) that the evolution of $\bar{x}$ is analogous to that of $\bar{\theta}$ and the difference between them varies slightly during shear for tests with a specified ϕ_μ. For the tests with different values of ϕ_μ, the evolutions of mean $\bar{x}$ and $\bar{\theta}$ are also very similar and their differences are kept almost constant when ϕ_μ is larger than 4°, as shown in Fig. 4(b). Here, we define the difference between $\bar{x}$ and $\bar{\theta}$ as δ, i.e.

$$\bar{x}=\bar{\theta}+\delta \tag{4}$$

The variation of the average angle δ against ϕ_μ corresponding to Fig. 4(b) is shown in Fig. 5 by open circular plots (○). It illustrates that δ increases with an increasing ϕ_μ in the lower range of ϕ_μ , but tends to be independent of ϕ_μ when ϕ_μ is larger than 4°. The fact that the evolution of the angle δ during shear varies slightly can also be supported by the results of the in-situ direct shear tests on various granular materials; this will be demonstrated in

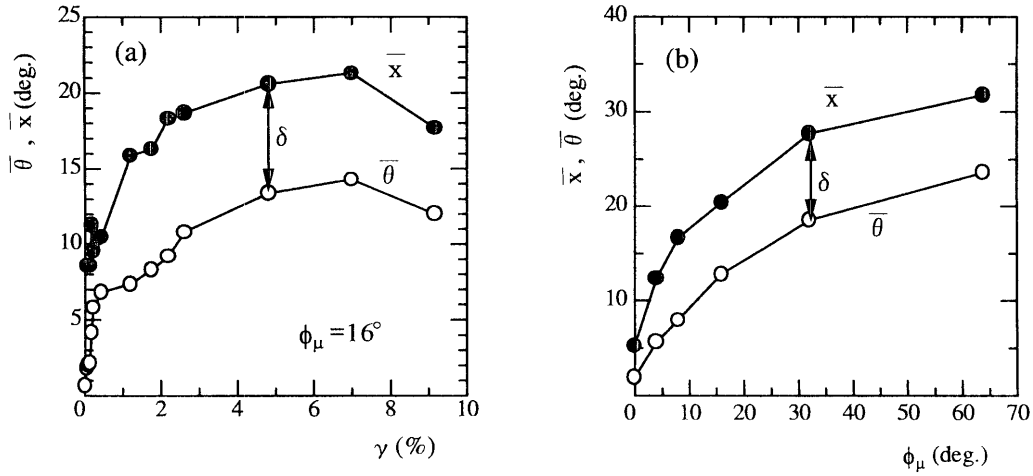

Fig. 4. Evolutions of $\bar{x}$ and $\bar{\theta}$ as well as δ in the simulated simple shear tests: (a) during shear corresponding to the specimen with $\phi_\mu=16°$, (b) with respect to different values of ϕ_μ. For each ϕ_μ, the plots refer to the mean values over the calculated shearing procedure.

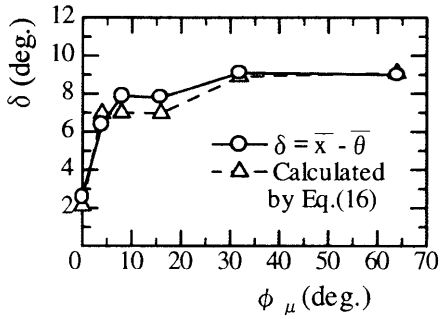

Fig. 5. Variation of δ against ϕ_μ

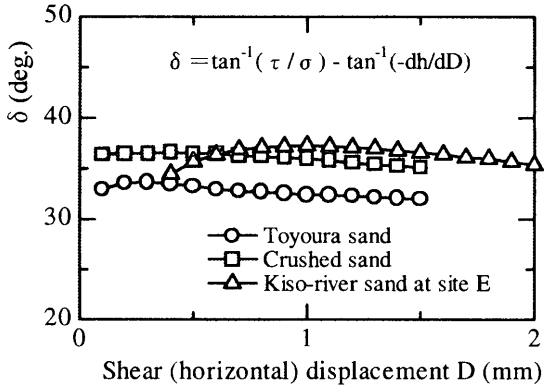

Fig. 6. Evolutions of the difference between the mobilized angle, $\tan^{-1}(\tau/\sigma)$, and the dilation angle, $\tan^{-1}(-dh/dD)$, during shear for Toyoura, crushed and Kiso-river sands obtained from the in-situ direct shear tests

the latter part of this paper. As an example, Fig. 6 shows the evolutions of the angles δ during shear for Toyoura, crushed and Kiso-river sands, where δ are calculated from the differences between the mobilized frictional angle and the dilation angle. Thus, for usual frictional granular materials, the difference δ can be assumed to be approximately constant during shear. Upon this assumption, the stress-dilatancy equation on the mobilized plane, namely, the relation between the shear-normal stress ratio, τ/σ_N, and the normal-shear strain increment ratio, $-d\varepsilon_N/d\gamma$, can be obtained through Eqs. (2), (3) and (4):

$$\frac{\tau}{\sigma_N} \cong \tan \bar{x} = \tan(\bar{\theta}+\delta) = \frac{\tan\bar{\theta}+\tan\delta}{1-\tan\bar{\theta}\cdot\tan\delta}$$
$$= \frac{1+\tan^2\delta}{1-\tan\bar{\theta}\cdot\tan\delta}\tan\bar{\theta}+\tan\delta$$
$$= \frac{1+\tan^2\delta}{1+\tan\delta\cdot\left(\frac{d\varepsilon_N}{d\gamma}\right)}\left(-\frac{d\varepsilon_N}{d\gamma}\right)+\tan\delta$$
$$= \lambda\left(-\frac{d\varepsilon_N}{d\gamma}\right)+\mu \qquad (5)$$

where $\lambda = \dfrac{1+\tan^2\delta}{1+\tan\delta\cdot\left(\dfrac{d\varepsilon_N}{d\gamma}\right)}$ and $\mu = \tan\delta$

The parameter λ varies with δ and $(-d\varepsilon_N/d\gamma)$, as

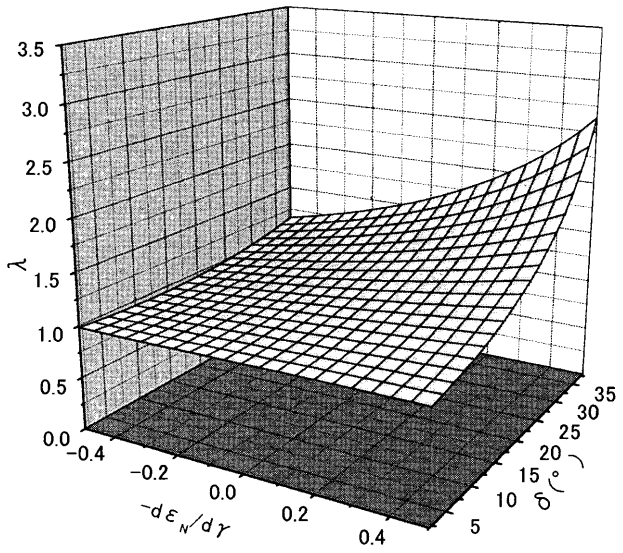

Fig. 7. Variation of λ with respect to δ and $-d\varepsilon_N/d\gamma$

shown in Fig. 7, but its variation is small in the lower range of δ. Since $\delta = \bar{x} - \bar{\theta}$, thereby both the probability distribution $F(x)$ of interparticle contact forces ($\bar{x}$, Eq. (2)) and the probability distribution $N(\theta)$ of interparticle contact angles ($\bar{\theta}$, Eq. (3)) are taken into consideration in the stress-dilatancy relation expressed by Eq. (5). If $F(x)$ is analogous to $N(\theta)$, and the mobilized interparticle friction angle $\phi_{\mu moi}$ for each contact is assumed to be equal to the average value of all contacts ($\bar{\phi}_{\mu mo}$), then $\bar{x}(=\overline{\theta_i+\phi_{\mu moi}})$ turns to be $(\bar{\theta}+\bar{\phi}_{\mu mo})$ and $\mu(=\tan\delta=\tan(\bar{x}-\bar{\theta}))$ turns to be $\tan\bar{\phi}_{\mu mo}$. In the previous study (Yamamoto et al., 1994), the parameter μ in Eq. (5) was equal to $\tan\bar{\phi}_{\mu mo}$.

Figures 8(a) and (b) show the τ/σ_N versus $\tan\bar{x}$ relationship and the $-d\varepsilon_N/d\gamma$ versus $\tan\bar{\theta}$ relationship on the mobilized plane under different values of ϕ_μ analyzed by using the numerically simulated data for the simple shear test with the stress-strain responses shown in Fig. 2, respectively. It is seen that Eqs. (2) and (3) bridge well the macroscopic variables (τ/σ_N, $-d\varepsilon_N/d\gamma$) with the microscopic variables ($\bar{x}$, $\bar{\theta}$) at different values of ϕ_μ. Figure 8(c) shows the stress-dilatancy relationship on the mobilized plane by combining Figs. 8(a) and (b), in which the straight line is drawn from Eq. (5) by using $\delta = 8°$ of the average value in Fig. 5 when ϕ_μ is larger than 4°. The experimental results represented by the black circular plots (●) are also given in Fig. 8(c). It is seen that the plots obtained from both the experiment and the numerical simulations are arranged very closely around the straight line drawn by Eq. (5), thus illustrating the reasonability of Eq. (5).

MICROSCOPIC INTERPRETATION FOR THE ANGLE δ

From the definition of $\delta = \bar{x} - \bar{\theta}$, the angle δ in the stress-dilatancy relationship of Eq. (5) is related to both the probability distribution $N(\theta)$ of interparticle contact

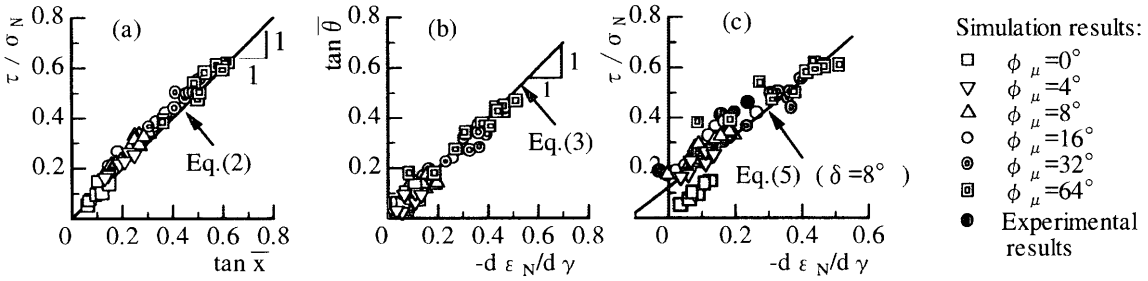

Fig. 8. Validation of Eqs. (2), (3) and (5) using the numerically simulated and experimental data for a simple shear test

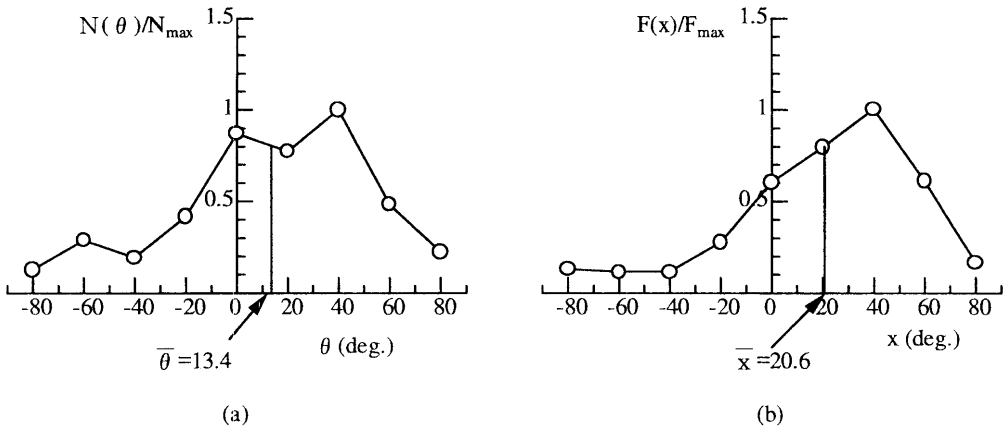

Fig. 9. Normalized probability distributions of contact angles $N(\theta)$ and total contact forces $F(x)$ along the mobilized plane at $\gamma=4.8\%$ corresponding to Fig. 4(a)

angles and the probability distribution $F(x)$ of interparticle contact forces. Figures 9(a) and (b) show the normalized probability distributions of $N(\theta)$ and $F(x)$ respectively along the mobilized plane at $\gamma=4.8\%$ in Fig. 4(a). Clearly, the normalized $N(\theta)$ and $F(x)$ are unsymmetrical about θ and x. But, $F(x)$ is more inclined toward the positive zone of x than $N(\theta)$ toward the positive zone of θ, leading to a larger value of $\bar{x}$ than that of $\bar{\theta}$ as shown in Fig. 9. Thus, the angle δ is qualitatively considered to result from the difference between $F(x)$ and $N(\theta)$.

Then, we examine quantitatively the value of the angle δ. As $x_i=\theta_i+\phi_{\mu moi}$, we rewrite the expression of $\bar{x}$ as follows:

$$\bar{x}=\frac{\sum_{i=1}^{n} f_i\cdot x_i}{\sum_{i=1}^{n} f_i}=\frac{\sum_{i=1}^{n} f_i\cdot(\theta_i+\phi_{\mu moi})}{\sum_{i=1}^{n} f_i}=\frac{\sum_{i=1}^{n} f_i\cdot\theta_i}{\sum_{i=1}^{n} f_i}+\frac{\sum_{i=1}^{n} f_i\cdot\phi_{\mu moi}}{\sum_{i=1}^{n} f_i}$$

$$=\frac{\int_{-\pi/2}^{\pi/2} F(\theta)\cdot\theta d\theta}{\int_{-\pi/2}^{\pi/2} F(\theta)d\theta}+\frac{\int_{-\pi/2}^{\pi/2} F(\theta)\cdot\phi_{\mu mo}(\theta)d\theta}{\int_{-\pi/2}^{\pi/2} F(\theta)d\theta}$$

$$=\bar{x}(\theta)+\bar{x}(\phi_{\mu mo}) \qquad (6)$$

where $F(\theta)$ and $\phi_{\mu mo}(\theta)$ represent the probability distributions of interparticle contact forces and the mobilized interparticle friction angles with respect to the contact angle θ along the mobilized plane, respectively. Then, we examine separately the two terms of $\bar{x}(\theta)$ and $\bar{x}(\phi_{\mu mo})$ in the right side of Eq. (6):

$$\text{About}\quad \bar{x}(\theta)=\frac{\int_{-\pi/2}^{\pi/2} F(\theta)\cdot\theta d\theta}{\int_{-\pi/2}^{\pi/2} F(\theta)d\theta}$$

From Fig. 9, we can obtain the distribution of the average interparticle contact forces against contact angle θ, which is designated by $f(\theta)$ and shown in Fig. 10. It is seen from Fig. 10 that $f(\theta)$ can be approximated with a straight line and this straight line is inclined upwards the positive zone of the contact angle ($\theta>0$), i.e. the distribution of the average interparticle forces $f(\theta)$ is biased toward the shearing direction. We express this straight line by

$$f(\theta)=f_0+k\theta \qquad (7)$$

where f_0 and k are the intercept and the slope of the straight line, respectively. It has been found that Eq. (7) is acceptable during the total shearing procedure for any cases of our DEM simulations as shown in Fig. 2(b). If the contact force at each contact point is assumed to be a constant (Matsuoka, 1974; Yamamoto, 1995), then this straight line will become horizontal with $k=0$. Figure 10 suggests that the interparticle contact forces along the shearing direction are larger on average than those against the shearing direction (with $\theta<0$), as illustrated in Fig. 11.

On the other hand, Matsuoka and Takeda (1980) approximated the probability distribution $N(\theta)$ in Fig. 9(a) with a triangular distribution that was expressed as

$$\left.\begin{aligned} N(\theta)&=\frac{h(\theta+\pi/2)}{\theta_p+\pi/2} \quad (-\pi/2\le\theta\le\theta_p)\\ N(\theta)&=\frac{h(\theta-\pi/2)}{\theta_p-\pi/2} \quad (\theta_p\le\theta\le\pi/2)\end{aligned}\right\} \tag{8}$$

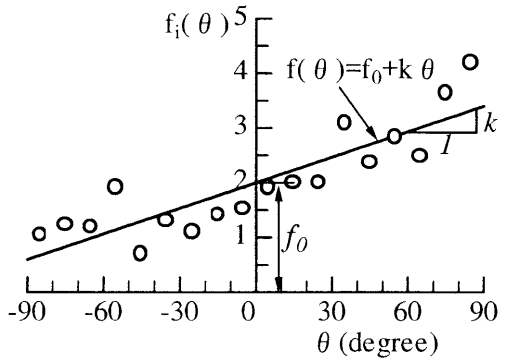

Fig. 10. Probability distribution of the average interparticle contact forces $f(\theta)$ plotted by using the data in Fig. 9

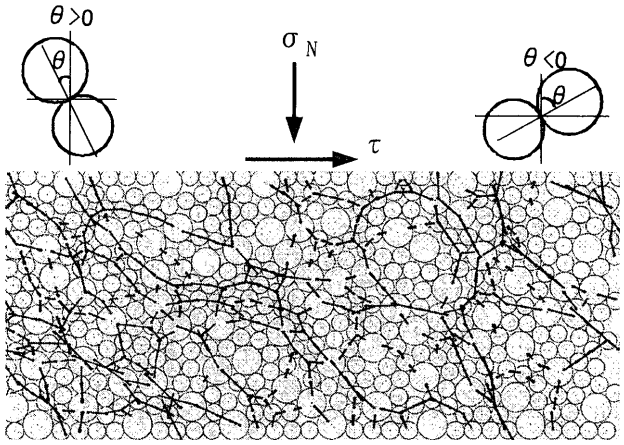

Fig. 11. Interparticle contact forces at $\gamma=4.8\%$ in Fig. 4(a), illustrating larger contact forces along the shear direction than against the shear direction

where h and θ_p denote the height and the contact angle at the peak of the triangular distribution, respectively.

Therefore, for a specific contact angle θ, the probability distribution $F(\theta)$ of the total interparticle contact forces is the product of the average interparticle contact force $f(\theta)$ multiplied by the number of the contacts $N(\theta)$, as shown in Fig. 12. It is expressed as

$$F(\theta)=f(\theta)\cdot N(\theta)=(f_0+k\theta)\cdot N(\theta) \tag{9}$$

By using Eqs. (8) and (9), one can easily obtain the following equation.

$$\bar{x}(\theta)=\frac{\int_{-\pi/2}^{\pi/2}F(\theta)\cdot\theta d\theta}{\int_{-\pi/2}^{\pi/2}F(\theta)d\theta}=\frac{\bar{\theta}+\dfrac{k}{f_0}\left(1.5\bar{\theta}^2+\dfrac{\pi^2}{24}\right)}{1+\dfrac{k}{3f_0}\bar{\theta}} \tag{10}$$

where $\bar{\theta}$ is the average value of the interparticle contact angles along the mobilized planes. It is further found from the DEM simulation results that the value of $(k/3f_0)\bar{\theta}$ is negligible ($\ll 1.0$). Thus, Eq. (10) can be approximated to be

$$\bar{x}(\theta)\cong\bar{\theta}+\frac{k}{f_0}\left(1.5\bar{\theta}^2+\frac{\pi^2}{24}\right) \tag{11}$$

About $\bar{x}(\phi_{\mu mo})=\dfrac{\int_{-\pi/2}^{\pi/2}F(\theta)\cdot\phi_{\mu mo}(\theta)d\theta}{\int_{-\pi/2}^{\pi/2}F(\theta)d\theta}$

Yamamoto (1995) simulated a biaxial compression test on aluminum rod assemblies by DEM, and found that the probability distribution of the mobilized interparticle friction angles on the mobilized plane, $\phi_{\mu mo}(\theta)$, is proportional to the distribution of the shear-normal stress ratio, $\tau(\theta)/\sigma(\theta)$, on the contact plane, which was expressed as

$$\frac{\phi_{\mu mo}(\theta)}{\phi_\mu}=c\cdot\frac{\tau(\theta)}{\sigma(\theta)}=c\cdot\frac{\sin\phi_{mo}\cos(2\theta-\phi_{mo})}{1+\sin\phi_{mo}\sin(2\theta-\phi_{mo})} \tag{12}$$

(c: constant)

Figure 13 gives the probability distribution of $\phi_{\mu mo}(\theta)$ normalized by ϕ_μ at $\gamma=4.8\%$ corresponding to Fig. 4(a), in which the solid line is sketched by using Eq. (12). It is seen that the law expressed by Eq. (12) also holds in the case of the simple shear test although there are some scatters in the plots that may have resulted from the limita-

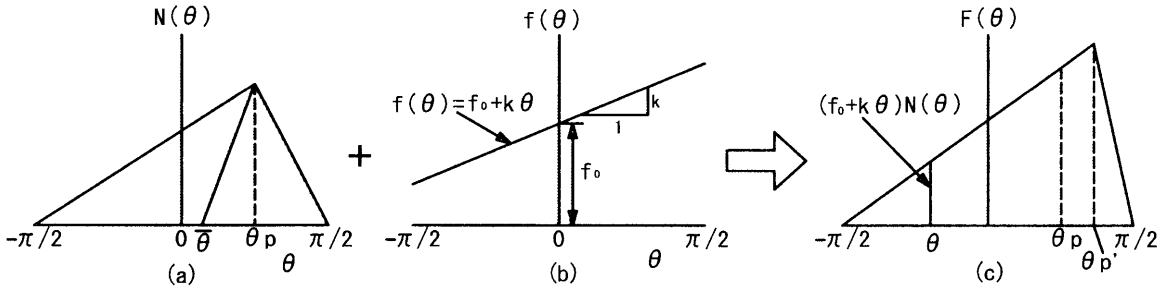

Fig. 12. Composition for the probability distribution of the total contact forces on mobilized plane: (a) Probability distribution of the contact angles, (b) Probability distribution of the average contact forces and (c) Probability distribution of the total contact forces

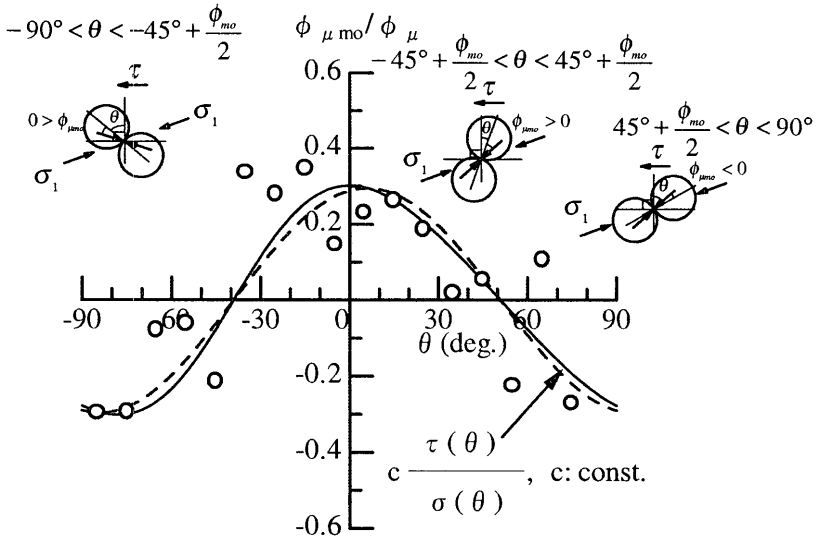

Fig. 13. Probability distribution of mobilized friction angles on mobilized plane at $\gamma = 4.8\%$ corresponding to Fig. 4(a)

tion of the particles in our DEM simulation. Here, the sign of the mobilized friction angle $\phi_{\mu mo}$ is taken as positive when the interparticle friction opposes the shear stress on the mobilized plane. From Eq. (12), we know that $\phi_{\mu mo}$ takes a positive value in the range of $-45° + \phi_{mo}/2 < \theta < 45° + \phi_{mo}/2$, and a negative one in the ranges of both $-90° < \theta < -45° + \phi_{mo}/2$ and $45° + \phi_{mo}/2 < \theta < 90°$ (*see* the upper illustrations in Fig. 13). Theoretically, the integration value of Eq. (12) in the range of $-90° < \theta < 90°$ is equal to zero. Therefore, Eq. (12) suggests that the particles comprising a granular media slide symmetrically along the shearing direction and against the shearing direction.

In order to simplify the integration calculation, we approximate Eq. (12) with the following form, which is shown by the broken line in Fig. 13:

$$\frac{\phi_{\mu mo}(\theta)}{\phi_{\mu}} \cong c' \cdot \cos(2\theta - \phi_{mo}) \quad (c': \text{constant}) \qquad (12)'$$

By using Eqs. (9) and (12)′, we can then obtain

$$\begin{aligned}\bar{x}(\phi_{\mu mo}) &= \frac{\int_{-\pi/2}^{\pi/2} F(\theta) \cdot \phi_{\mu mo}(\theta) d\theta}{\int_{-\pi/2}^{\pi/2} F(\theta) d\theta} \\ &= \frac{c' \phi_{\mu} \sin \phi_{mo} \cos 3\bar{\theta}}{\left(1 + \frac{k}{f_0}\bar{\theta}\right)\left(\frac{\pi^2}{4} - 9\bar{\theta}^2\right)} \left\{ \left(1 + \frac{3k}{f_0}\bar{\theta}\right) \cos(3\bar{\theta} - \phi_{mo}) \right. \\ &\quad \left. - \frac{k}{f_0} \sin(3\bar{\theta} - \phi_{mo}) \right\} \end{aligned} \qquad (13)$$

By using the numerically simulated data for the simple shear test with $\phi_{\mu} = 16°$ at shear strain $\gamma = 4.8\%$, the magnitude of $\bar{x}(\phi_{\mu mo})$ is calculated to be 0.2° from Eq. (13). It is found that the magnitudes of $\bar{x}(\phi_{\mu mo})$ are very small at other shear strains for the same test as well as for the other simulated tests with different values of ϕ_{μ}. This can be understood from the aforementioned fact that $\phi_{\mu mo}(\theta)$ takes both positive and negative values over the range of $-90° < \theta < 90°$ (*cf.* Fig. 13), and has a probability distribution as expressed by Eq. (12). Thus, the term $\bar{x}(\phi_{\mu mo})$ can be neglected, i.e. assuming

$$\bar{x}(\phi_{\mu mo}) \cong 0 \qquad (14)$$

Substituting Eqs. (11) and (14) into Eq. (6) yields the expression $\bar{x}$ of the average angle of the contact forces

$$\bar{x} = \bar{x}(\theta) + \bar{x}(\phi_{\mu mo}) \cong \bar{\theta} + \frac{k}{f_0}\left(1.5\bar{\theta}^2 + \frac{\pi^2}{24}\right) \qquad (15)$$

Finally, the angle δ can be approximately expressed as

$$\delta \cong \frac{k}{f_0}\left(1.5\bar{\theta}^2 + \frac{\pi^2}{24}\right) \qquad (16)$$

where $\bar{\theta}$ and f_0 are the average interparticle contact angle and the average interparticle contact force over all the contacts along the mobilized plane, respectively; and k is the slope of the straight line characterizing the distribution of the average interparticle contact force against the contact angle. The value of k/f_0 is positive, suggesting that the interparticle contact forces are inclined toward the shearing direction (contact angle $\theta > 0$) on average.

By using the numerically simulated data for the simple shear tests with the stress-strain responses as shown in Fig. 2 (b), we calculated the values of the angle δ at different shear strains under different values of ϕ_{μ} by using Eq. (16). The average δ for each ϕ_{μ} are plotted in Fig. 5 by open triangular plots (△), which agree well with the values (plots ○) obtained from its definition $\delta = \bar{x} - \bar{\theta}$. Therefore, Eq. (16) can predict reasonably the difference δ between $\bar{x}$ and $\bar{\theta}$.

INFLUENCES OF INTERPARTICLE SURFACE FRICTION, GRAIN SHAPE AND CONFINING PRESSURE

Influence of Interparticle Surface Friction

In order to investigate the influence of surface friction of grains on the stress-dilatancy relationship, we simulated the same simple shear test as shown in Fig. 1 by varying the values of ϕ_μ to be 0°, 4°, 8°, 16°, 32° and 64° while holding the other parameters necessary for the simulation constant. The simulated results with respect to the $\tau/\sigma \sim \gamma \sim \varepsilon_N$ relationships are presented in Fig. 2 and the corresponding stress-dilatancy relationships are illustrated in Fig. 8. The variation of the intercepts $\mu(=\tan\delta)$ against ϕ_μ are plotted in Fig. 5. It can be seen from Fig. 5 that the intercept μ increases with the increase in ϕ_μ in the lower range of ϕ_μ values, but it tends not to be sensitive to the interparticle friction angle ϕ_μ when ϕ_μ is larger than 4 °. It is known from Eq. (16) that the interparticle friction ϕ_μ is not directly related to the intercept $\mu(=\tan\delta)$; its effect on δ is reflected indirectly through the effects on $\bar{\theta}$, k and f_0. It is found from the numerically simulated data that the average contact angle $\bar{\theta}$ increases with the increase in ϕ_μ, being consistent with the increase in dilative normal strain of the sample; but, the ratio k/f_0 tends to be a certain value when ϕ_μ is larger than 4°, resulting in non-sensitivity of δ to ϕ_μ.

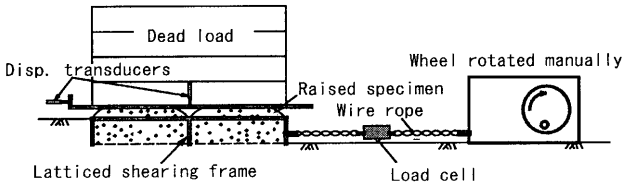

(a) Schematic view along the shear direction

(b) Tests on sands in laboratory

Fig. 14. A newly developed in-situ direct shear testing method. In laboratory, a specimen box is used to replace in-situ ground

Influence of Grain Shape

Figure 14 shows the schematic view of a newly developed in-situ direct shear testing method (Matsuoka et al., 1998, 2001). The influences of grain shapes on the stress-dilatancy relationship are investigated by carrying out a series of such direct shear tests on various granular materials including 5 sands sampled along the Kiso-river in Japan from the downstream to the upstream (Liu et al., 2002). The particle photographs of 5 Kiso-river sands are shown in Fig. 15, which are considered to represent the typical grain shapes of usual soils. The grain shape is

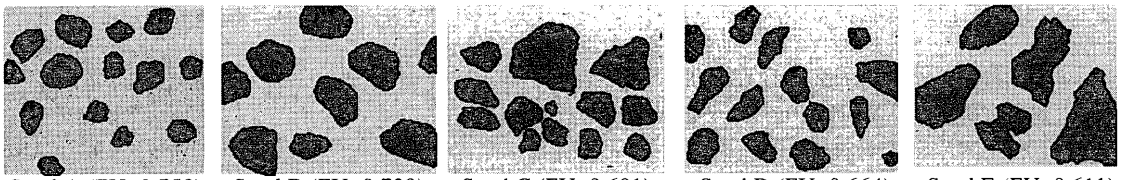

Fig. 15. Particle photographs of 5 sands sampled along Kiso-river from the downstream to the upstream

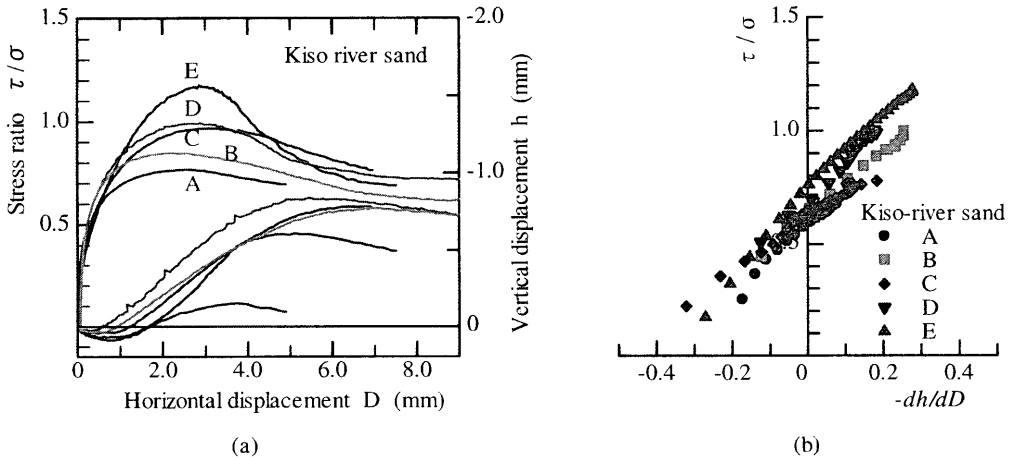

(a) (b)

Fig. 16. Results of the in-situ direct shear tests on 5 Kiso-river sands under a normal stress of 20 kPa and a relative density D_r of about 50%

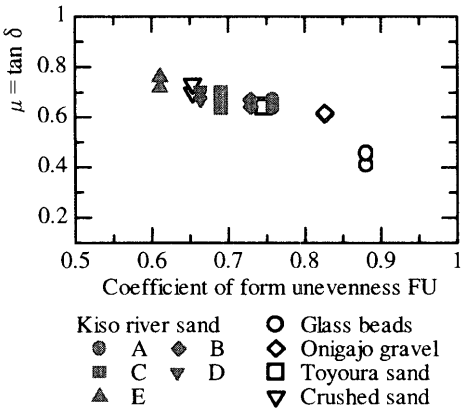

Fig. 17. Influences of grain shapes on the intercepts of the stress-dilatancy relationship obtained from the in-situ direct shear tests

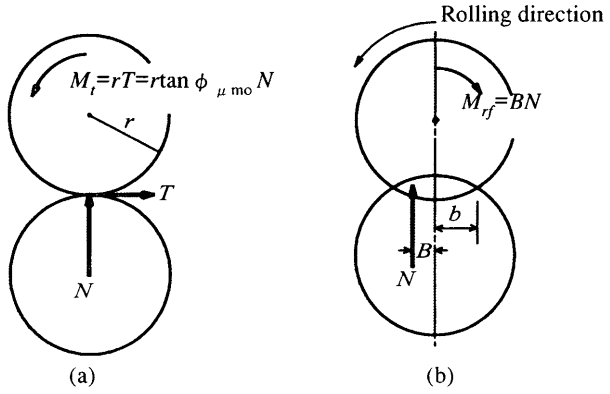

Fig. 18. Rolling moment due to sliding friction force and modeling of rolling resistance between two circular particles (after Sakaguchi et al., 1993; Yamamoto, 1997)

characterized with a coefficient of form unevenness FU that was originally proposed by Yoshimura (1994), and defined as $FU=(4\pi A)/L^2$, where A is the projected area of grain and L is the grain perimeter. For a sphere, $FU=1.0$; the more angular the grain is, the smaller the value of FU is. Figure 16(a) presents the relationships among shear-normal stress ratio τ/σ, horizontal displacement D and vertical displacement h for 5 Kiso-river sands under a normal stress of 20 kPa and a relative density D_r of about 50%. Figure 16(b) shows the relationship between shear-normal stress ratio, τ/σ, and vertical-horizontal displacement increment ratio, $-dh/dD$, up to the peak shear strength in accordance with Fig. 16(a). For the direct shear test, $-d\varepsilon_N/d\gamma=-(dh/L)/(dD/L)=-dh/dD$, where L = the thickness of the shear zone. These 5 Kiso-river sands have different grain shapes with values of FU ranging from 0.758 to 0.611, but they may be approximately considered to have the similar physical characteristics such as the surface friction of grains because they are sampled from the same river. It can be seen from Fig. 16 that the grain shape affects both the shear strength and the stress-dilatancy relationship. The more angular the grain is, the higher the shear strength is and the larger the intercept μ in the stress-dilatancy relationship is, too. Figure 17 presents the plots of the intercepts μ against the coefficient of form unevenness FU for all tests on these 5 Kiso-river sands and other granular materials such as glass beads, Toyoura sand, Onigajo gravel and crushed sand. It is seen that the intercept μ increases when the grain becomes angular (decreases in FU), and its variation is about 0.1 for 5 Kiso-river sands. For glass beads, the value of the intercept μ is much lower (about 0.1) than that for other materials, probably resulting from the extremely low value of the surface friction.

Then, we investigate how the grain shape contributes to the intercept $\mu(=\tan\delta)$ in the stress-dilatancy relationship by using the numerically simulated results for the same simple shear test as shown in Fig. 1. As we know, angular grains are interlocked well and have a great resistance to particle rolling in a granular media. Thus, in our simulation, we introduce a moment of resisting particle rolling between particles to model the effect of grain shape qualitatively. Such a simulation method was originally proposed by Sakaguchi et al. (1993), and has been implemented by Yamamoto (1997) to study the effect of grain shape qualitatively on the internal friction angle of granular materials. Figure 18 shows the rolling moment due to the sliding friction force between two circular particles and the modeling of rolling resistance by introducing a moment, M_{rf}, which is given by

$$M_{rf}=BN \tag{17}$$

where B is the width with a maximum value of half of the pressed contact width, and N is the normal force acting on the particle contact. The particles begin to roll when the rolling moment due to the sliding friction, $M_t=r\tan\phi_{\mu mo}N$, exceeds the rolling resistance moment, M_{rf}. By comparing Eq. (17) with the sliding frictional law $F=\mu N$, the width B is also termed as a frictional coefficient against the rolling by Sakaguchi et al. (1993). In this paper, the degree of grain angularity is modeled by changing the value of B. Figure 19 shows the DEM simulated results for the same simple shear test as shown in Fig. 1 with $B/r=0$ and 0.02, where r is the radius of particle. It is seen that both the shear strength and the intercept μ increase when the rolling resistance moment is introduced between particles ($B/r=0.02$), which models qualitatively the influences of the grain shapes on the shear strength and the intercept μ as observed by experiments (Fig. 16). Other researchers have also obtained similar results from DEM simulation by combining several smaller circular particles into clusters to model a larger angular particle (e.g. Kuwabara and Maeda, 2000). Our simulated results illustrate that both $\bar{\theta}$ and k/f_0 increase when a moment of resisting particle rolling between particles is introduced, suggesting that grain shape contributes to the increase of the average contact angle $\bar{\theta}$ between particles on the mobilized plane and causes interparticle forces to be more inclined toward the shearing direction. Therefore, granular media consisting of more angular grains have a larger intercept μ for the stress-dilatancy relationship expressed in Eq. (5).

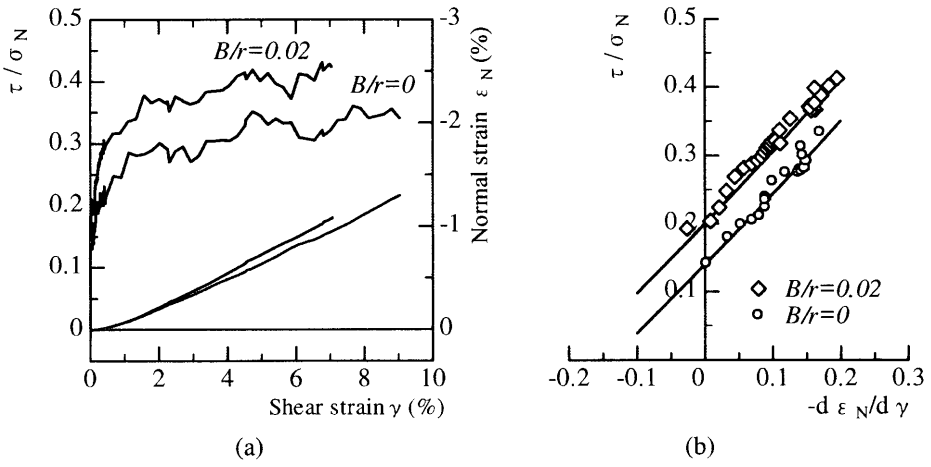

Fig. 19. DEM simulation results for the same simple shear test as shown in Fig. 1 with and without rolling resistance moment between particles

Influences of Confining Pressures

In this argument, we assume that the fabric structure of a granular media remains unchanged when the granular media is subjected to different confining pressures. That is to say, the probability distribution of contact angles $N(\theta)$ and thereafter the average contact angle $\bar{\theta}$ do not change under different confining pressures. Commonly, the interparticle forces corresponding to any contact angle increase approximately in proportion to the increase in the confining pressure. Figure 20 illustrates a schematic view for the probability distribution of average interparticle force $f(\theta)$ against contact angle θ, when the subjected confining pressure doubles. It can be understood from Fig. 20 that the ratio of f_0/k holds constant when the granular media is subjected to different confining pressures. Therefore, it can be inferred from Eq. (16) that the intercept $\mu(=\tan\delta)$ in the stress-dilatancy relationship is not affected by subjected confining pressures.

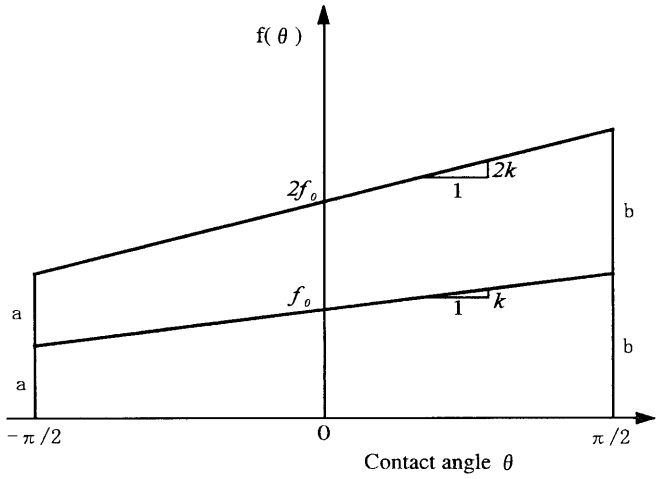

Fig. 20. Variation for the distribution of average interparticle force $f(\theta)$ against contact angle θ when the confining pressure doubles

RELATIONSHIP BETWEEN SHEAR-NORMAL STRESS RATIO AND VERTICAL-HORIZONTAL DISPLACEMENT INCREMENT RATIO FOR VARIOUS GRANULAR SOILS OBTAINED FROM A NEW IN-SITU DIRECT SHEAR TEST

As stated above, the intercept $\mu(=\tan\delta)$ in the stress-dilatancy relationship depends weakly on the interparticle friction angle ϕ_μ except in the low range of ϕ_μ, and is independent of the confining pressure. But, it is affected to some extent by the grain shapes. For 5 sands sampled along the Kiso-river from downstream to upstream, which generally represent the typical grain shapes of usual soil materials, the variation of the intercept $\mu(=\tan\delta)$ induced by grain shape is found to be about 0.1, corresponding to a variation in the angle δ about $4\sim5°$. These findings are also supported by experimental results of the newly developed large-sized in-situ direct shear tests on various coarse-grained granular soils (rockfill materials). Figure 21 shows this new in-situ direct shear test at a construction site of embankment using the same principle as illustrated in Fig. 14(a). Up to now, such tests have been performed on various coarse-grained granular soils with quite different grain sizes and rock classifications.

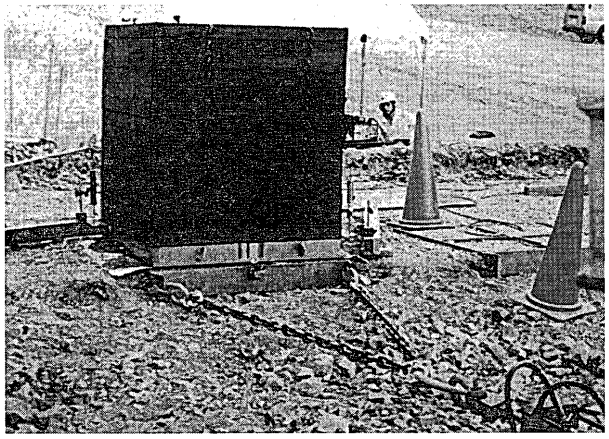

Fig. 21. Large in-situ direct shear test on coarse granular soils at site *N*

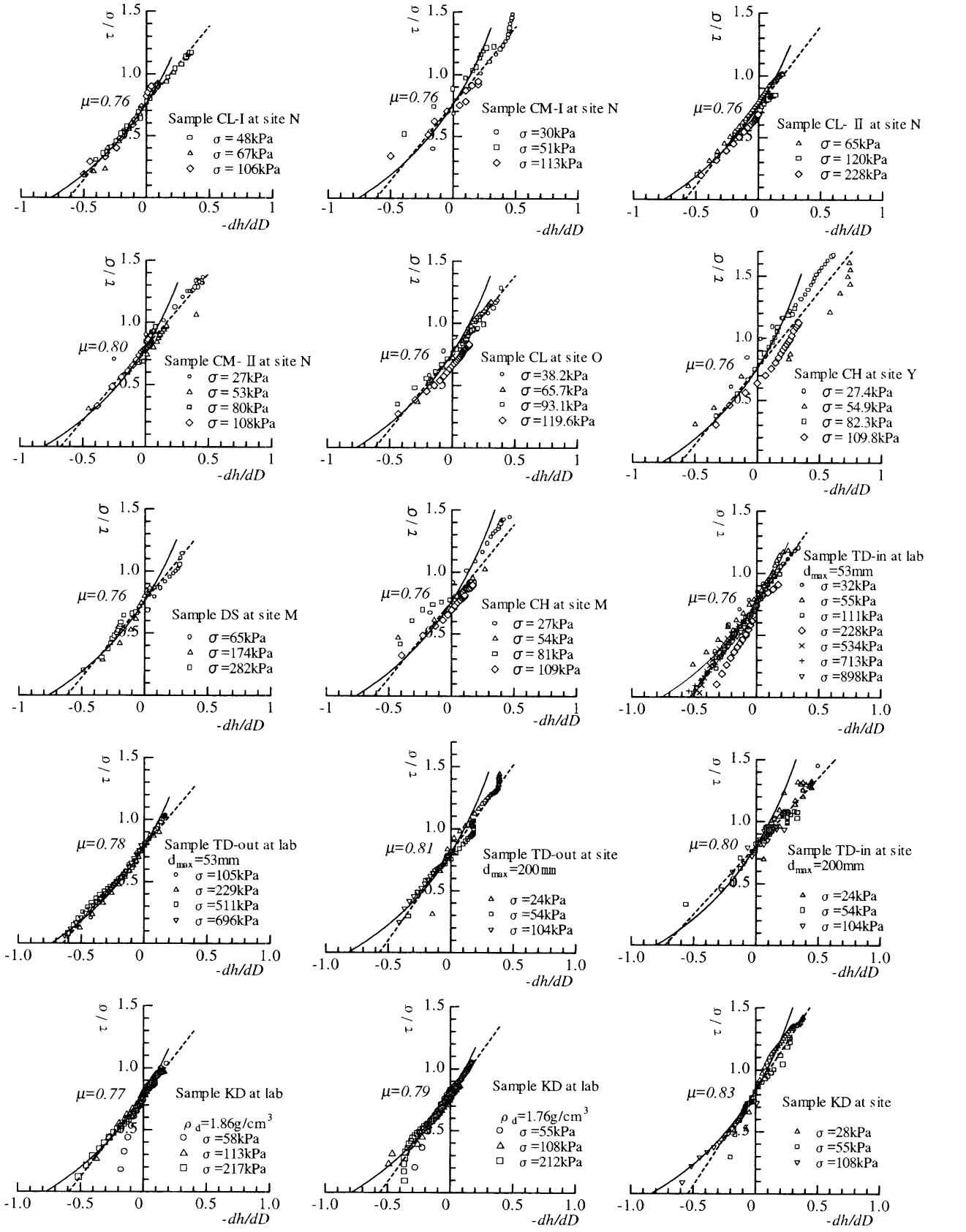

Fig. 22. Relationship between shear-normal stress ratio, τ/σ, and vertical-horizontal displacement increment ratio, $-dh/dD$, up to peak strength for various coarse granular soils obtained from large-sized in-situ direct shear tests

Figure 22 summarizes the obtained results with respect to the relationship between the shear-normal stress ratio, τ/σ, and the vertical-horizontal displacement increment ratio, $-dh/dD$, up to the peak shear strength. It has been mentioned that, for the direct shear test, $-dh/dD$ is equivalent to the normal-shear strain increment, $-d\varepsilon_N/d\gamma$, in the stress-dilatancy relationship expressed by Eq. (5). In Fig. 22, the broken straight lines are drawn from the test data for each sample by the least squares method, while the solid curves are drawn from Eq. (5) by using the respective intercepts as shown in Fig. 22. Some discrepancies between the theoretical solid lines and the experimental plots are considered to result from both measurement accuracies and approximations of Eq. (2). The downward convex solid curves are due to the change of the parameter λ in Eq. (5) with $-d\varepsilon_N/d\gamma$. However, based on the experimental results in Fig. 22, it might be acceptable to assume a constant λ (*e.g.* Matsuoka et al., 1974, 1980, 1994), i.e. assume a linear stress-dilatancy relationship. Nevertheless, it can be seen from Fig. 22 that the intercepts vary slightly (from 0.76 to 0.83) for the tested samples in spite of quite large differences in grain sizes, rock classifications and so on. These experimental results justify the arguments in this paper.

CONCLUDING REMARKS

In this paper, based on DEM simulation results for a simple shear test, a stress-dilatancy relation of granular materials on the mobilized plane derived by Matsuoka (1974), $\tau/\sigma_N=\lambda(-d\varepsilon_N/d\gamma)+\mu$, is reviewed from a microscopic view point by taking the real interparticle contact force and the mobilized interparticle friction angle for each contact into consideration. The macro-variables, τ/σ_N and $-d\varepsilon_N/d\gamma$, on the mobilized plane are related to the average angle $\bar{x}$ of the interparticle contact force to the normal of the mobilized plane, expressed by Eq. (2), and the average interparticle contact angle $\bar{\theta}$, expressed by Eq. (3), respectively. There exists a difference δ between $\bar{x}$ and $\bar{\theta}$, which is interpreted as

$$\delta=\frac{k}{f_0}\left(1.5\bar{\theta}^2+\frac{\pi^2}{24}\right)$$

where f_0 is the average interparticle contact force of all the contacts and k is the slope of the straight line that characterizes the probability distribution of the average interparticle contact force against the contact angle. The ratio of k/f_0 represents the biased degree of the probability distribution of the interparticle contact forces to the positive zone of θ (along the shear direction). The intercept μ in the stress-dilatancy relationship is considered to be equal to $\tan\delta$. It is found that the angle δ depends weakly on the interparticle friction angle ϕ_μ except in the lower range of ϕ_μ and is independent of the confining pressure. However, it is affected to some extent by grain shapes.

ACKNOWLEDGEMENTS

The authors express their sincere gratitude to Dr. S. Yamamoto of Obayashi Corporation for his great help in the DEM simulation. They are also grateful to Mr. S. Satoh, Mr. T. Shinozaki and Mr. T. Yamada, former and current Master students of Nagoya Institute of Technology, for their assistance in the experimental laboratory work.

REFERENCES

1) Cundall, P. A. and Strack, O. D. L. (1979): A discrete numerical model for granular assemblies, *Géotechnique*, **29** (2), 47–65.
2) Kuwabara, N. and Maeda, K. (2000): Processes of development and disappearance of micro-structure in granular materials with different grain properties by distinct element method, *J. of Applied Mechanics*, JSCE, **3**, 469–480 (in Japanese).
3) Liu, S. H. (1999): Development of a new in-situ direct shear test method and its application to problems of slope stability and bearing capacity, *Dr. Eng. Thesis*, Nagoya Institute of Technology.
4) Liu, S. H. and Matsuoka, H. (2001): A microscopic study on stress-dilatancy relationship of granular materials by DEM, *Powers and Grains 2001* (ed. by Kishino), Balkema, 207–211.
5) Liu, S. H., Matsuoka, H., Yamada, T. and Shigeno, M. (2002): Influences of grain shape and surface friction on a stress-dilatancy relationship, *Proc. of 37th Japan National Conf. on Geotechnical Engineering*, 433–434.
6) Matsuoka, H. (1974): A microscopic study on shear mechanism of granular materials, *Soils and Foundations*, **14** (1), 29–43.
7) Matsuoka, H. and Nakai, T. (1974): Stress-deformation and strength characteristics of soil under three different principal stresses, *Proc. of JSCE*, (232), 59–70 (in Japanese).
8) Matsuoka, H. and Takeda, K. (1980): A stress-strain relationship for granular materials derived from microscopic shear mechanism, *Soils and Foundations*, **20** (3), 45–58.
9) Matsuoka, H. and Yamamoto, S. (1994): A microscopic study on shear mechanism of granular materials by DEM, *J. of Geotech. Engrg.*, JSCE, (487/III-26), 167–175 (in Japanese).
10) Matsuoka, H. and Liu, S. H. (1998): Simplified direct box shear test on granular materials and its application to rockfill materials, *Soils and Foundations*, **38** (4), 275–284.
11) Matsuoka, H., Liu, S. H., Sun, D. A. and Nishikata, U. (2001): Development of a new in-situ direct shear test, *Geotech. Testing J.*, GTJODJ, **24** (1), 92–102.
12) Nakai, T. and Matsuoka, H. (1980): A unified law for soil shear behavior under three dimensional stress condition, *Proc. of JSCE*, (303), 65–71 (in Japanese).
13) Rowe, P. W. (1962): Stress-dilatancy relation for static equilibrium of an assembly of particles in contact, *Proc. Roy. Soc.*, (A-269), 500–527.
14) Sakaguchi, H., Ozaki, E. and Igarashi, T. (1993): Plugging of the flow of granular materials during the discharge from a silo, *Int. J. of Modern Physics*, **B7**, 1949–1963.
15) Scofield, A. N. and Wroth, C. P. (1968): *Critical State Soil Mechanics*, London McGrawHill.
16) Yamamoto, S. (1995): Fundamental study on mechanical behavior of granular materials by DEM, *Dr. Eng. Thesis*, Nagoya Institute of Technology (in Japanese).
17) Yamamoto, S. (1997): Study on effect of rolling resistance between particles on the internal friction angle of granular materials by DEM, *Proc. of 32th Japan National Conf. on Geotech. Engrg.*, 497–498 (in Japanese).
18) Yoshimura, Y. (1994): Effect of grain shape on primary and secondary characteristics of granular materials such as sands, *Dr. Eng. Thesis*, Nagaoka Univ. of Sci. Technology (in Japanese).